

Achieving high-efficient triboelectric nanogenerators by suppressing electrostatic breakdown effect

Yikui Gao,^{‡ab} Di Liu,^{‡ab} Yanhong Li,^a Jiaqi Liu,^a Linglin Zhou,^{ab} Xinyuan Li,^{ab} Zhihao Zhao,^{ab} Shaoxin Li,^{ab} Peiyuan Yang,^{ab} Zhong Lin Wang,^{*ac} Jie Wang^{*ab}

^aBeijing Institute of Nanoenergy and Nanosystems, Chinese Academy of Sciences, Beijing 101400, P.R. China.

^bSchool of Nanoscience and Technology, University of Chinese Academy of Sciences, Beijing 100049, P.R. China.

^cSchool of Materials Science and Engineering, Georgia Institute of Technology, Atlanta, 30332, USA

[‡]Y. Gao and D. Liu contributed equally to this work.

*Corresponding Author: J. Wang: wangjie@binn.cas.cn; Z. L. Wang: zhong.wang@mse.gatech.edu

This file includes:

Supplementary Figures:

Supplementary Figure 1. The energy cycle of CS-TENG.

Supplementary Figure 2. The analytical solution of the COMSOL Multiphysics simulation software.

Supplementary Figure 3. The motion path of CS-TENG.

Supplementary Figure 4. Physical images of the mechanical switch.

Supplementary Figure 5. The relationship between charge density and voltage of CS-TENG at contact state with different film thicknesses.

Supplementary Figure 6. The relationship between C_T , C_{air} and C_d .

Supplementary Figure 7. The relationship between separation distance and transferred charge.

Supplementary Figure 8. The relationship of parasitic capacitor and CS-TENG.

Supplementary Figure 9. The LC circuit and corresponding simulated results.

Supplementary Figure 10. Inductor selection.

Supplementary Figure 11. Capacitance selection.

Supplementary Figure 12. The output current of CS-TENG after PMC when C_{out} is 2.2 μF .

Supplementary Figure 13 The maximum energy cycle and maximum average power of CS-TENG.

Supplementary Figure 14. Output performance of CS-TENG after PMC with different charge densities.

Supplementary Figure 15. The energy output of CS-TENG after PMC with different dielectric thicknesses.

Supplementary Figure 16. The electric circuit with or without LC circuit.

Supplementary Figure 17. Output performance of CS-TENG with PMC at different frequencies.

Supplementary Figure 18. The stability of CS-TENG continuously working for 10 000 cycles with PMC.

Supplementary Figure 19. The working voltage when CS-TENG drives 100 LEDs.

Supplementary Notes:

Supplementary Note 1. HV-LQ and LV-HQ energy cycle of CS-TENG.

Supplementary Note 2. The voltage across the air gap of CS-TENG.

Supplementary Note 3. The maximum surface charge density (σ_{\max}) of the CS-TENG.

Supplementary Note 4. Surface charge density when CS-TENG operates in open-circuit condition.

Supplementary Note 5. The charge-transfer efficiency of CS-TENG.

Supplementary Note 6 The influence of parasitic capacitors on CS-TENG.

Supplementary Note 7 The influence of inductor on LC circuit

Supplementary Note 8 The methods of calculating energy conversion efficiency

Supplementary Note 9. The specific working process of LC circuit.

Supplementary Table:

Supplementary Table 1. Comparison of Performance of TENG and corresponding PMC

Supplementary Table 2. The parameters in CS-TENG for simulation

Supplementary Table 3 The resistance of electronic components

Supplementary Videos:

Supplementary Video 1. The simulation results of potential difference during the contact process and separation process of CS-TENG under 0 M Ω .

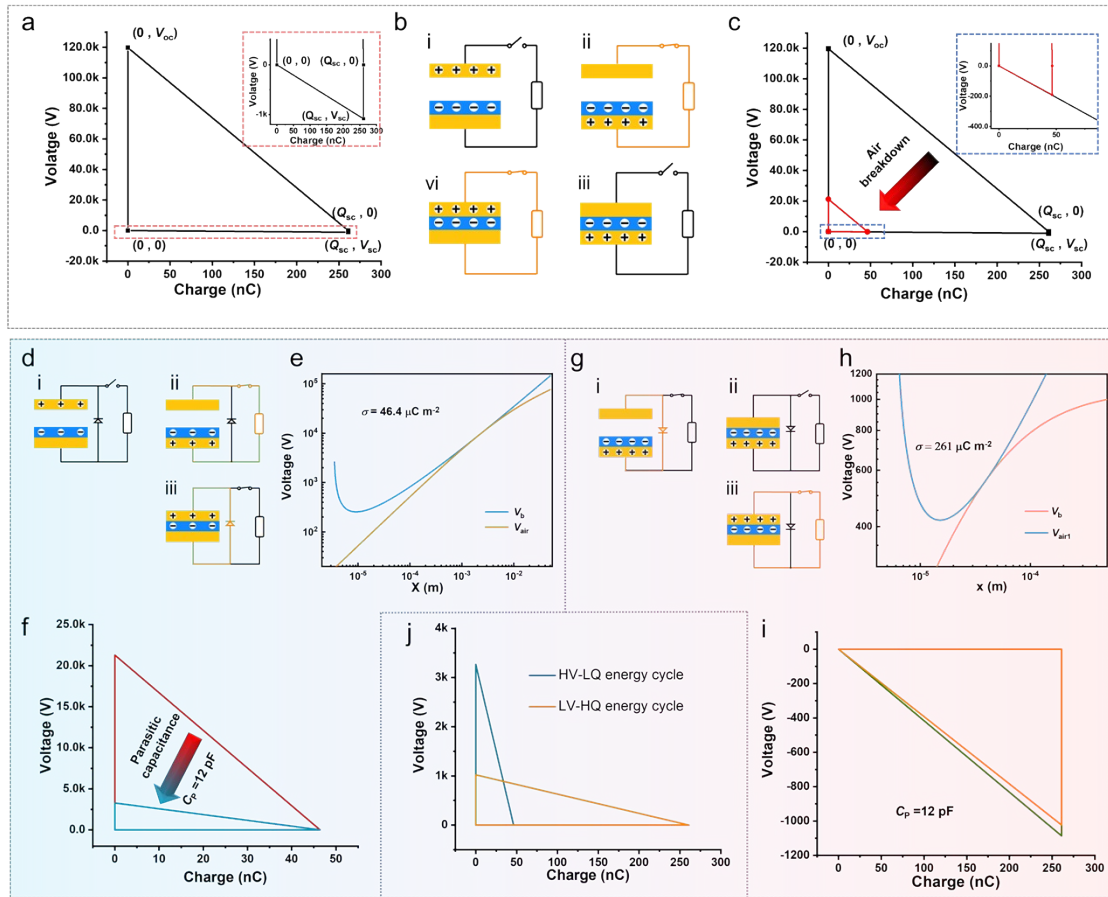
Supplementary Video 2. The simulation results of potential difference during the contact process and separation process of CS-TENG under 20 M Ω .

Supplementary Video 3. CS-TENG drives 100 LEDs without flashing.

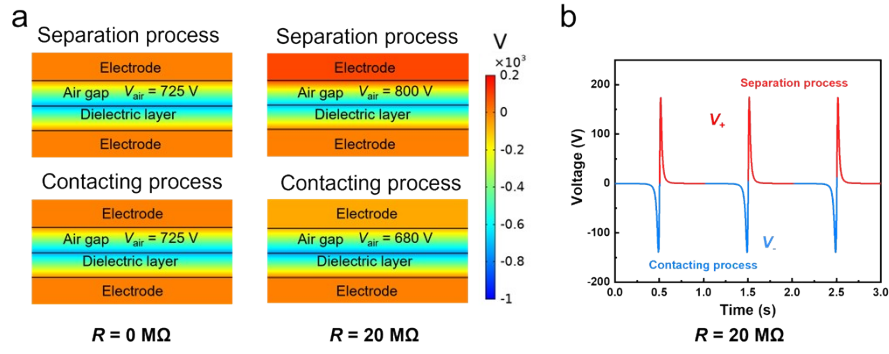
Supplementary Video 4. CS-TENG drives 100 LEDs with flashing.

Supplementary Video 5. CS-TENG drives 6 hygrometers at 2.5 Hz.

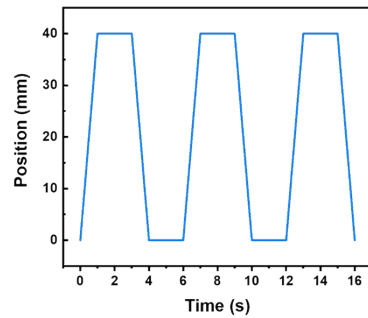
Supplementary Video 6. CS-TENG drives buzzer.



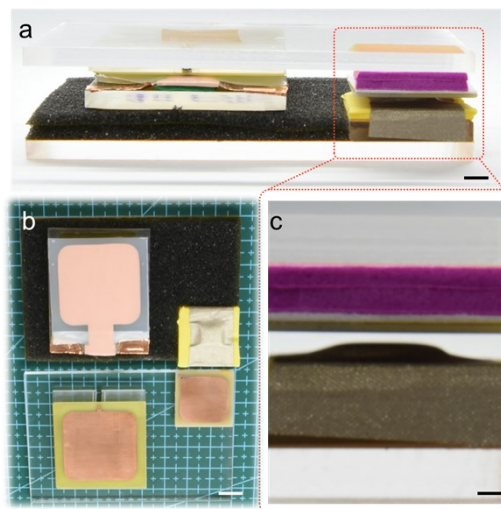
Supplementary Figure 1. The energy cycle of CS-TENG. **a** The ideal maximum energy cycle of the CS-TENG. **b** The working process of the ideal maximum energy cycle. **c** The theoretical maximum energy cycle of the CS-TENG after electrostatic breakdown. **d** The working process of maximum energy cycle of CS-TENG with half-wave circuit (-). **e** The surface charge density of at open-circuit condition. **f** The energy cycle (blue curve) of the CS-TENG with parasitic capacitance (15 pF). **g** The working process of maximum energy cycle of CS-TENG with half-wave circuit (+). **h** The surface charge density of at short-circuit condition. **i** The energy cycle (orange curve) of the CS-TENG with parasitic capacitance (15pF). **j** The HV-LQ energy cycle and LV-HQ energy cycle.



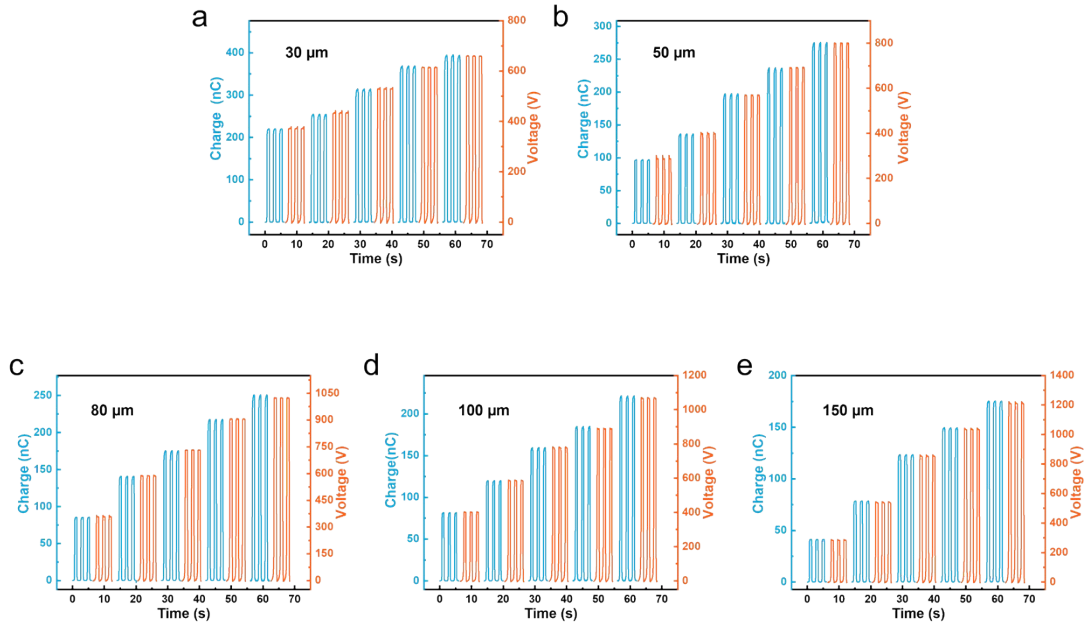
Supplementary Figure 2. a The simulation results of potential during the contacting process and separation process of CS-TENG with 0 M Ω or 20 M Ω . **b** The simulation results of output voltage when the resistance is 20 M Ω .



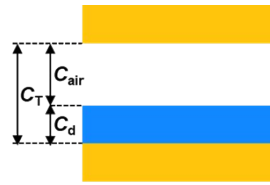
Supplementary Figure 3. The motion path of CS-TENG.



Supplementary Figure 4. Physical images of the mechanical switch. a Side view (scale bar: 5 mm); **b** top view (scale bar: 10 mm); **c** the air gap (scale bar: 2 mm).

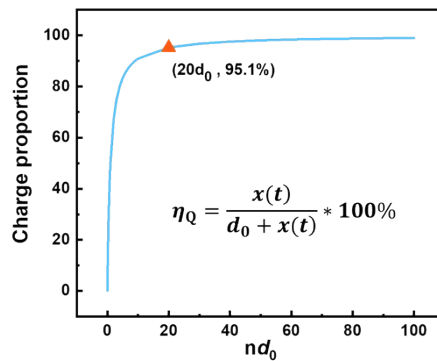


Supplementary Figure 5. a-e The relationship between charge density and voltage of CS-TENG at contact state with different film thicknesses. **a** 30 μm , **b** 50 μm , **c** 80 μm , **d** 100 μm and **e** 150 μm .

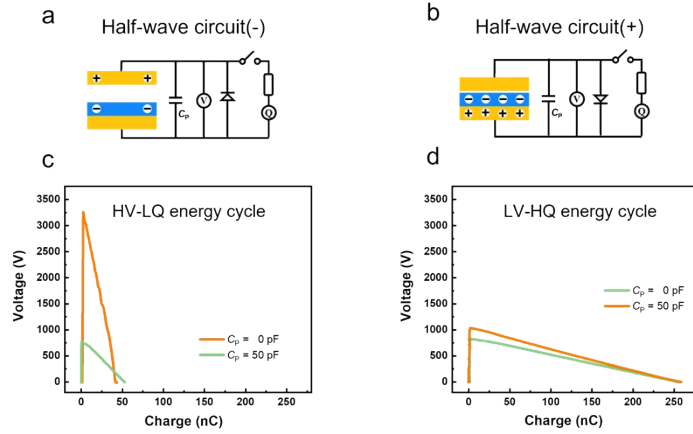


$$C_T = \frac{C_{\text{air}} C_d}{C_{\text{air}} + C_d}$$

Supplementary Figure 6. The relationship between C_T , C_{air} and C_d .

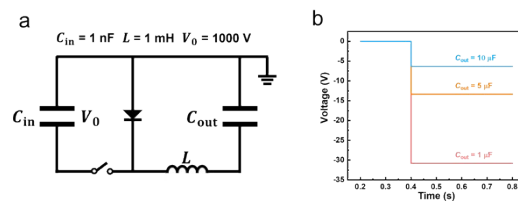


Supplementary Figure 7. The relationship between separation distance and transferred charge. d_0 is the ratio of the thickness (d) and the dielectric constant of dielectric film (ϵ_r).



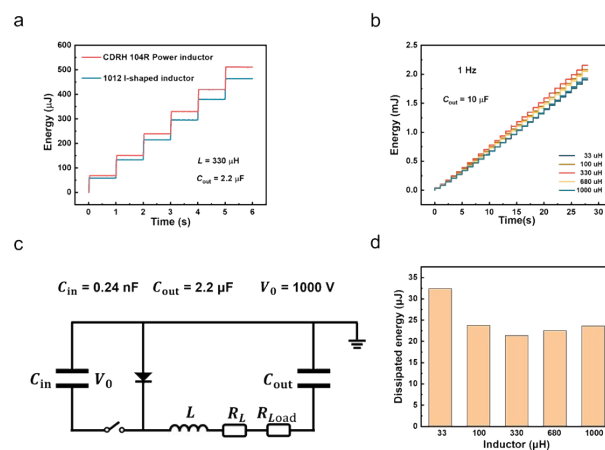
Supplementary Figure 8. The relationship of parasitic capacitor and CS-TENG.

The circuit of testing **a** HV-LQ energy cycle and **b** LV-HQ energy cycle. The influence of parasitic capacitor on **c** HV-LQ energy cycle and **d** LV-HQ energy cycle.



Supplementary Figure 9. The LC circuit and corresponding simulated results. a

Parameters of the LC circuit. **b** The output voltage with different capacitances.

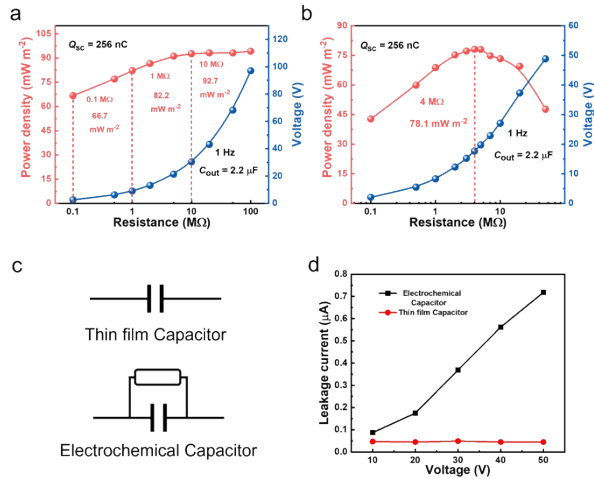


Supplementary Figure 10. Inductor selection. a The comparison of final energy

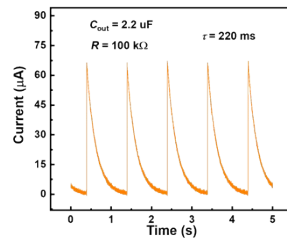
output when L is magnetic shielded inductance or non-magnetic shielded inductance. **b**

The comparison of energy output when the inductance is different. **c** Parameters of the

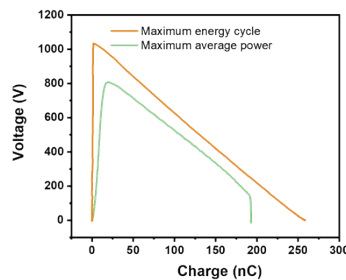
LC circuit. **d** The dissipated energy on the resistors.



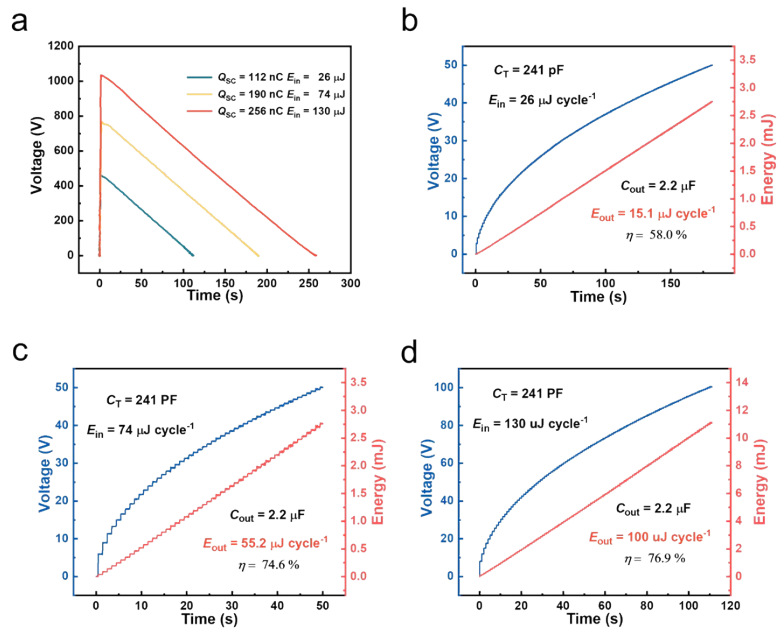
Supplementary Figure 11. Capacitance selection. **a** The power density and voltage of CS-TENG after PMC with the film capacitor. **b** The power density and voltage of CS-TENG after PMC with the electrochemical capacitor. **c** Equivalent circuit diagram of film capacitor and electrochemical capacitor. The electrochemical capacitor can be regarded as an ideal capacitor and a resistor in parallel. **d** The leakage current of film capacitors and electrochemical capacitor.



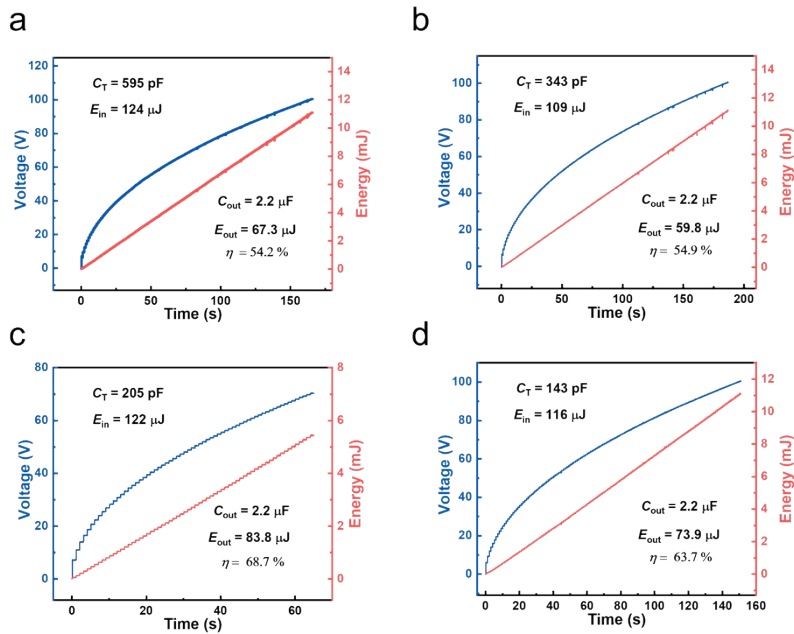
Supplementary Figure 12. The output current of CS-TENG after PMC when C_{out} is $2.2 \text{ }\mu\text{F}$.



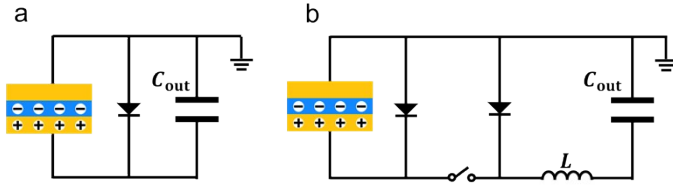
Supplementary Figure 13 The maximum energy cycle and maximum average power of CS-TENG.



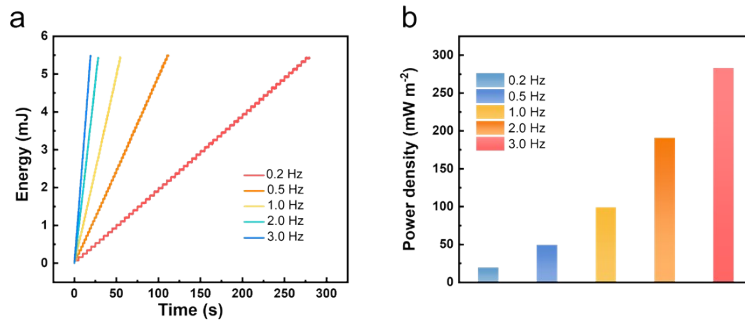
Supplementary Figure 14. Output performance of CS-TENG after PMC with different charge densities. **a** Energy output of CS-TENG with different surface charge densities before PMC. The energy output of CS-TENG after PMC when Q_{SC} is **b** 113 nC, **c** 190 nC and **d** 256 nC.



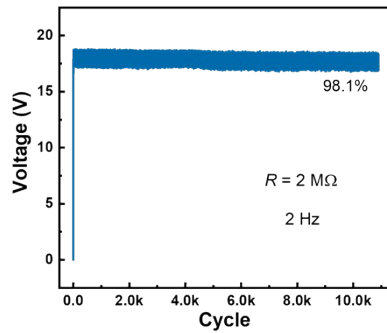
Supplementary Figure 15. The energy output of CS-TENG after PMC with different dielectric thicknesses. **a** 30 μm , **b** 50 μm , **c** 100 μm and **d** 150 μm .



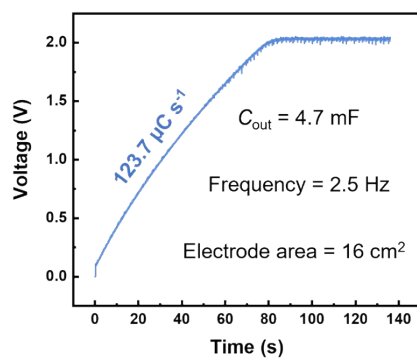
Supplementary Figure 16. The electric circuit with or without LC circuit. a without LC circuit; b with LC circuit.



Supplementary Figure 17. Output performance of CS-TENG with PMC at different frequencies. a Output energy and b output power density.



Supplementary Figure 18. The stability of CS-TENG continuously working for 10 000 cycles with PMC.



Supplementary Figure 19. The working voltage when CS-TENG drives 100 LEDs.

Supplementary Note 1 HV-LQ and LV-HQ energy cycle of CS-TENG

Starting from the cycle for maximized energy output (CMEO)¹, we explore how to achieve the maximum energy cycle of CS-TENG in practical applications. Supplementary Fig. 1a is the theoretical maximum energy cycle of CS-TENG, and the working process is shown in Supplementary Fig. 1b. However, the theoretical value could not be obtained in the atmosphere due to electrostatic breakdown (Supplementary Fig. 1c). Compared with the energy output obtained at separating process of CS-TENG, the energy output of CS-TENG at contacting process is basically negligible (The inset of Supplementary Fig. 1c).

Based on that, we can simplify the method of achieving the maximized energy cycle by introducing the half-wave circuit (-) (Supplementary Fig. 1d), and the theoretical value of charge density can be calculated based on the Paschen's law (Supplementary Note 4), which is below $50 \mu\text{C m}^{-2}$ (Supplementary Fig. 1e). Meanwhile, the energy cycle will be reduced again due to the parasitic capacitance in the test circuit. Therefore, the general actual maximum energy cycle that can be utilized is shown in the Supplementary Fig. 1f.

In addition, we can also achieve the maximum energy cycle by introducing the half-wave circuit (+) (Supplementary Fig. 1g). According to the previous conclusion, the surface charge density would be stable at σ_{max} . We can also calculate theoretical σ_{max} based on the Paschen's law (Supplementary Note 3), which is related with the film thickness (Supplementary Fig. 1h). It is worth noting that the energy cycle does not decrease much even considering the parasitic capacitance (Supplementary Fig. 1i).

Considering the characteristics of these two energy cycles, we call them HV-LQ energy cycle and LV-HQ energy cycle respectively (Supplementary Fig. 1j). They all feature high energy output, but HV-LQ energy cycle has been studied in detail in other works. Therefore, in the following work, we will formulate a power management strategy around the LV-HQ energy cycle.

Supplementary Note 2 The voltage across the air gap of CS-TENG

According to Gauss's theorem (ignoring edge effect), the electric field across the air gap (E_{air}) can be described as:

$$E_{air} = \frac{\sigma S - Q}{S\epsilon_0} \quad (1)$$

The electric field across the dielectric film (E_d) is:

$$E_d = \frac{-Q}{S\epsilon_r\epsilon_0} \quad (2)$$

Therefore, the potential difference between two electrodes (V_{12}) is:

$$V_{12} = E_{air}x + E_d d \quad (3)$$

where σ represents the surface charge density, S , d , x and ϵ_r is the area, thickness, air gap and relative dielectric constant of the dielectric film respectively.

1. If the external load resistance is zero, V_{12} will be zero, as following:

$$V_{12} = 0 \quad (4)$$

According to equation (3), the Q can be calculated as:

$$Q = \frac{S\sigma x}{d_0 + x} \quad (5)$$

$$d_0 = \frac{d}{\epsilon_r} \quad (6)$$

Combining equation (1), (5) and (6), the potential difference across the air gap is:

$$V_{air1} = \frac{\sigma d_0 x}{(d_0 + x)\epsilon_0} \quad (7)$$

2. If the external load resistance is not zero, there will be a potential difference between the two electrodes. The voltage on the resistance can be calculated by the COMSOL Multiphysics simulation (**Fig. S2b**), and the corresponding parameters of simulation is shown in **Table S2**. When CS-TENG moves from contact to separation, positive voltage will be built on the resistance according to the direction of current. V_{12} can be described as the following equation:

$$V_{12} = V_+ \quad (8)$$

According to equation (3), the Q can be calculated as:

$$Q = \frac{S(\sigma x - V_+ \varepsilon_0)}{d_0 + x} \quad (9)$$

Combining formula (1) and (9), the potential difference across the air gap is:

$$V_{air2} = \frac{(\sigma d_0 + V_+ \varepsilon_0)x}{(d_0 + x)\varepsilon_0} \quad (10)$$

When CS-TENG moves from separation to contact, negative voltage will be built on the resistance according to the direction of current. V_{12} can be described as the following equation:

$$V_{12} = V_- \quad (11)$$

According to formula (3), the Q can be calculated as:

$$Q_{SC} = \frac{S(\sigma x - V_- \varepsilon_0)}{d_0 + x} \quad (12)$$

Combining formula (1) and (12), the potential difference across the air gap is:

$$V_{air3} = \frac{(\sigma d_0 + V_- \varepsilon_0)x}{(d_0 + x)\varepsilon_0} \quad (13)$$

By comparing formula (7), (10) and (13), the following relationship will be built:

$$V_{air2} > V_{air1} > V_{air3} \quad (14)$$

Under short-circuit condition, the maximum surface charge density (σ_{\max}) of CS-TENG with different thickness of dielectric films can be calculated (Supplementary Note 3). By introducing σ_{\max} into formula (7), (10) and (13), the corresponding voltage can be calculated as shown in Supplementary Fig. 2b. It is clearly that the curves of V_{air1} and V_b are tangent, and the curves of V_{air2} intersects V_b , and the curves of V_{air3} separates from V_b .

Supplementary Note 3 The maximum surface charge density (σ_{max}) of the CS-TENG

According to Paschen's law:

$$V_b = \frac{APx}{\ln(Px) + B} \quad (15)$$

where A and B are the constants determined by the composition and the pressure of the gas. In standard atmosphere condition, A and B are $2.774 \times 10^7 \text{ V atm}^{-1} \text{ m}^{-1}$ and 12.2, respectively.

When $V_{air} \leq V_b$ always holds, the electrostatic breakdown in the gap will not occur. Therefore, the maximum surface charge density should satisfy the following equation by combining equation (7) and (15):

$$\sigma_{max} \leq \left(\frac{AP\varepsilon_0(d_0 + x)}{(\ln(Px) + B)d_0} \right)_{min} \quad (16)$$

Here, we define the function $f(x, d_0)$ as:

$$f(x, d_0) = \frac{AP\varepsilon_0(d_0 + x)}{(\ln(Px) + B)d_0} \quad (17)$$

Thus, the partial derivative of $f(x, d_0)$ with respect to x can be described as the following equation:

$$\frac{df(x, d_0)}{dx} = \frac{\ln(Px) + B - \frac{d_0 + x}{x}}{[\ln(Px) + B]^2 d_0} \quad (18)$$

When $\frac{df(x, d_0)}{dx}$ is zero, the following equation will be satisfied:

$$d_0 = x \ln(Px) + Bx - x \quad (19)$$

From the equation (16) and (19), the σ_{max} of different d_0 can be obtained.

Supplementary Note 4 Surface charge density when CS-TENG operates in open-circuit condition

The approximate formula of parallel plate capacitor in non-ideal case is:

$$C_{(x)} = \varepsilon_0 \varepsilon_r \left\{ \frac{lw}{x} + \frac{l}{\pi} \right\} [1 + \ln] \quad (20)$$

Here, l (32 mm) and w (32 mm) are length and width of the electrodes. Given that there is no charge transfer between electrodes of CS-TENG in open-circuit condition, the potential difference across the air gap (V_{air}) is:

$$V_{air} = \frac{lw\sigma}{C(x)} \quad (21)$$

Combining equation (20) and (21), the potential difference across the air gap can be obtained. When $V_{air} \leq V_b$, the electrostatic breakdown will not happen. Therefore, the maximum surface charge density (σ_{max}) in open circuit can be calculated to be $46.4 \mu\text{C m}^{-2}$, as shown in Supplementary Fig 1e.

Supplementary Note 5 The charge-transfer efficiency of CS-TENG

According to equation (5), the transferred charges (Q) of CS-TENG in short-circuit can be expressed as:

$$Q = \frac{S\sigma x}{d_0 + x} \quad (22)$$

where S is the contact area and σ is the surface charge density of film, and d_0 is defined as the ratio of film' thickness d to relative permittivity ϵ_r , and x is the distance between top electrode and film. The ratio of transferred charges of TENG in external circuit to total charges is defined as charge transfer efficiency (η_Q), as shown below:

$$\eta_Q = \frac{x}{d_0 + x} * 100\% \quad (23)$$

As shown in Supplementary Fig. 5, η_Q can reach to 95.1% when x is 20 times of d_0 , which indicates that this method is superior for harvesting low-amplitude mechanical energy.

Supplementary Note 6 The influence of parasitic capacitors on CS-TENG

As many previous works reported, the parasitic capacitor in practical circuits is usually a parallel connected capacitor to the circuit with the value between 0 and 10 pF, and it also can reach up to hundreds of pF in some cases². In our work, we mainly consider the common condition where the value of parasitic capacitance is between 0 and 50 pF. To quantitatively studying the effect of parasitic capacitor on the performance of output power of the CS-TENG in the LV-HQ energy cycle and in the HV-LQ energy cycle, an additional commercial capacitor which is parallel connected with the CS-TENG is employed to play the role of parasitic capacitor. The output voltage of CS-TENG during the maximum energy cycle measurement can be calculated as:

$$V_{OC} = \frac{Q_{SC}}{C_T + C_P} \quad (24)$$

The energy can be derived as:

$$E_T = \frac{V_{OC}Q_{SC}}{2} = \frac{Q_{SC}^2}{2(C_T + C_P)} \quad (25)$$

Therefore, the energy of CS-TENG with large C_T is insensitive to the parasitic capacitor.

Supplementary Note 7 The influence of inductor on LC circuit

Theoretically, the output performance is not affected by the inductor if the resistance of the LC circuit is zero. However, in practical conditions, the resistance of each component in the circuit is not zero. The resistance of the inductor (R_L) can be obtained from the handbook, and the resistance of other electronic components (R_{Load} includes the resistance of the diode and wire.) can be measured by a precision source. The results are presented in Supplementary Table 3.

We have calculated the dissipated energy on the resistors by a simulation software (LTspice). The circuit diagram is shown in Supplementary Fig. 10c. The simulated results indicate that the dissipated energy in the circuit is smallest when the inductance is 330 μH (Supplementary Fig. 10d). In addition, the experimental results also demonstrate that the inductance of 330 μH can produce the highest output energy (Supplementary Fig. 10b). Therefore, based on experimental and simulated results, we chose the inductor of 330 μH for the subsequent experiments.

Supplementary Note 8 The methods of calculating energy conversion efficiency

We calculated the energy efficiency by two methods in this work. One is calculated by the maximum average power of CS-TENG on the resistor before and after the PMC, which indicates the change in output power. The other one is calculated by stored energy per cycle in C_{in} and C_{out} (In this work, the maximum energy cycle of CS-TENG is the stored energy per cycle in C_T), which indicates the energy conversion efficiency of PMC. Generally, the output energy calculated by the maximum average power is less than the value by the maximum energy cycle (Supplementary Fig. 13), because the charge cannot completely transfer through the large resistance. Therefore, the energy conversion efficiency calculated by the first method is larger than the value calculated by the second method.

Supplementary Note 9 The specific working process of LC circuit

The specific working process of LC circuit is shown in Fig. 4b:

In the first step (Fig. 4b i), TENG converts mechanical energy into electrical energy and stores electrical energy in its internal capacitor after a working cycle. We assume that when $t = 0$, the initial voltage value of C_T is V_0 , and the initial voltage of C_{out} is 0.

In the second step, the switch is turned on and C_T is used as a power source, as shown in Fig. 4b ii. The corresponding current direction and voltage direction are also marked (There is no current flow due to one-way electric conduction of diode.).

According to Kirchhoff's voltage law:

$$V_T + V_L + V_{out} = 0 \quad (26)$$

We assume that transferred charge of C_T is Q , so V_T , L and C_{out} can be expressed as:

$$V_T = \frac{C_T V_0 - Q}{C_T} \quad (27)$$

$$V_L = -L \frac{d^2 Q}{dt^2} \quad (28)$$

$$V_{out} = -\frac{Q}{C_{out}} \quad (29)$$

Therefore:

$$V_T = \frac{d^2 Q}{dt^2} + \frac{Q}{L} \left(\frac{1}{C_T} + \frac{1}{C_{out}} \right) \quad (30)$$

According to initial condition $Q(t=0) = 0$, $I(t=0) = dQ/dt = 0$, the solution of differential equation is:

$$Q(t) = -\frac{V_0 C_T C_{out}}{C_T + C_{out}} \cos \left(\sqrt{\frac{C_T + C_{out}}{L C_T C_{out}}} t \right) + \frac{V_0 C_T C_{out}}{C_T + C_{out}} \quad (31)$$

Therefore, the current of the loop and the voltage of C_T , L and C_{out} is:

$$I(t) = \frac{dQ}{dt} = V_0 \sqrt{\frac{C_{out} C_T}{L(C_T + C_{out})}} \sin \left(\sqrt{\frac{C_T + C_{out}}{L C_T C_{out}}} t \right) \quad (32)$$

$$V_T(t) = V_0 + \frac{V_0 C_{out}}{C_T + C_{out}} \cos\left(\sqrt{\frac{C_T + C_{out}}{LC_T C_{out}}} t\right) - \frac{V_0 C_{out}}{C_T + C_{out}} \quad (33)$$

$$V_{out}(t) = -\frac{V_0 C_T}{C_T + C_{out}} \cos\left(\sqrt{\frac{C_T + C_{out}}{LC_T C_{out}}} t\right) + \frac{V_0 C_T}{C_T + C_{out}} \quad (34)$$

$$V_L(t) = V_0 \cos\left(\sqrt{\frac{C_T + C_{out}}{LC_T C_{out}}} t\right) \quad (35)$$

$$t \in \left[0, \frac{\pi}{2} \sqrt{\frac{LC_T C_{out}}{C_T + C_{out}}}\right] \quad (36)$$

When $t_1 = \frac{\pi}{2} \sqrt{\frac{LC_T C_{out}}{C_T + C_{out}}}$, the second process is over. If C_{out} is significantly larger than C_T , and $V_T = V_{out} \approx 0$ as well as $V_L = 0$, the current will reach the maximum.

In the third step, L serves as power source for energy release and the diode is turned on. The directions of corresponding current and voltage direction are shown in Fig. 4b iii. Similarly, according to Kirchhoff's voltage law:

$$V_L + V_{out} = 0 \quad (37)$$

The voltage of L and C_{out} can be expressed as:

$$V_L = -L \frac{d^2 Q}{dt^2} \quad (38)$$

$$V_{out} = -\frac{Q}{C_{out}} \quad (39)$$

Therefore:

$$\frac{d^2 Q}{dt^2} + \frac{Q}{LC_{out}} = 0 \quad (40)$$

Considering the initial condition $Q(t-t_1 = 0) = 0$, $I(t-t_1 = 0) = dQ/dt =$

$V_0 \sqrt{\frac{C_{out}C_T}{L(C_T + C_{out})}}$, the solution of differential equation is:

$$Q(t) = V_T C_{out} \sqrt{\frac{C_T}{C_T + C_{out}}} \sin \left(\sqrt{\frac{1}{LC_{out}}}(t - t_1) \right) \quad (41)$$

Therefore:

$$V_{out}(t) = -V_0 \sqrt{\frac{C_T}{C_T + C_{out}}} \sin \left(\sqrt{\frac{1}{LC_{out}}}(t - t_1) \right) \quad (42)$$

$$I(t) = V_0 \sqrt{\frac{C_{out}C_T}{L(C_T + C_{out})}} \cos \left(\sqrt{\frac{1}{LC_{out}}}(t - t_1) \right) \quad (43)$$

When $t - t_1 = \frac{\pi}{2} \sqrt{LC_{out}}$, the third process ends.

Given that C_T is a constant, V_{out} will depend on the C_{out} . Here, a simulation result is shown in Supplementary Fig. 7. Supplementary Fig. 7a is the parameter of the LC circuit. V_{out} will gradually decrease with increasing of the C_{out} (Supplementary Fig. 7b).

Supplementary Table 1 Comparison of Performance of TENG and corresponding PMC

No.	Maximized energy Yes/No	Matching C_{in} [*] Yes/No	Area (cm ²)	Voltage (V)	Average power (mW m ⁻² Hz ⁻¹)		Power efficiency (%)	Energy output (mJ m ⁻² cycle ⁻¹)		Energy efficiency (%)	Refs
					TENG	PMC		TENG	PMC		
1	No	No	36	359	—	—	—	6.3	2.2	35.0%	3
2	No	No	48	374	9.7	7.0	71.9%	9.7	2.8	29.6%	4
3	No	Yes	104	2050	5.6	4.1	73.6%	—	—	—	5
4	No	Yes	32	500	27.4	23.1	84.3%	—	—	—	6
5	No	Yes	32	590	—	32.2	—	—	—	—	7
6	No	Yes	28	650	30.8	26.1	84.8%	50.8	33.9	65.0%	8
7	Yes	Yes	100	6000	109.0	89.0	81.6%	108.0	98.0	90.7%	9
8	Yes	No need	10	1020	95.4	92.4	97.1%	130.0	100.0	76.9%	This work

*A suitable capacitor is necessary for TENG to obtain the high energy output in most of previous works.

Supplementary Table 2 The parameters in CS-TENG for simulation

Area (cm ²)	10
Air gap (mm)	$x = 4.92 \sin(2\pi t)$
Permittivity of vacuum (ϵ_0)	8.854×10^{-12}
Relative permittivity of PTFE (ϵ_r)	2.2
Thickness of PTFE (μm)	80
Surface charge density ($\mu\text{C m}^{-2}$)	261

Supplementary Table 3 The resistance of electronic components

L	R_L	R_{Load}
33 μH	93 m Ω	1010 m Ω
100 μH	304 m Ω	1010 m Ω
330 μH	1090 m Ω	1010 m Ω
680 μH	2200 m Ω	1010 m Ω
1000 μH	3100 m Ω	1010 m Ω

References

1. Y. Zi, S. Niu, J. Wang, Z. Wen, W. Tang and Z. L. Wang, *Nat. Commun.*, 2015, **6**, 8376.
2. K. Dai, X. Wang, S. Niu, F. Yi, Y. Yin, L. Chen, Y. Zhang and Z. You, *Nano Res.*, 2017, **10**, 157-171.
3. H. Zhang, F. Marty, X. Xia, Y. Zi, T. Bourouina, D. Galayko and P. Basset, *Nat. Commun.*, 2020, **11**, 3221.
4. X. Cheng, L. Miao, Y. Song, Z. Su, H. Chen, X. Chen, J. Zhang and H. Zhang, *Nano Energy*, 2017, **38**, 438-446.
5. W. Yan, Y. Liu, P. Chen, L. N. Y. Cao, J. An, T. Jiang, W. Tang, B. Chen and Z. L. Wang, *Adv. Energy Mater.*, 2022, **12**, 2103677.
6. W. Harmon, D. Bamgboje, H. Guo, T. Hu and Z. L. Wang, *Nano Energy*, 2020, **71**, 104642.
7. W. Harmon, H. Guo, D. Bamgboje, T. Hu and Z. L. Wang, *Nano Energy*, 2021, **85**, 105956.
8. Z. Cao, Z. Wu, R. Ding, S. Wang, Y. Chu, J. Xu, J. Teng and X. Ye, *Nano Energy*, 2022, **93**, 106891.
9. Z. Wang, Q. Tang, C. Shan, Y. Du, W. He, S. Fu, G. Li, A. Liu, W. Liu and C. Hu, *Energy Environ. Sci.*, 2021, **14**, 6627-6637.